ORIGINAL ARTICLE

CNS Neuroscience & Therapeutics Open Access WILEY

Spike-and-wave discharges of absence seizures in a sleep waves-constrained corticothalamic model

Martynas Dervinis | Vincenzo Crunelli ⓘ

Neuroscience Division, School of Bioscience, Cardiff University, Museum Avenue, Cardiff, CF10 3AX, UK

Correspondence
Martynas Dervinis and Vincenzo Crunelli, Neuroscience Division, School of Bioscience, Cardiff University, Museum Avenue, Cardiff CF10 3AX, UK.
Email: martynas.dervinis@gmail.com and crunelli@cardiff.ac.uk

Present address
Martynas Dervinis, School of Physiology, Pharmacology and Neuroscience, Biomedical Building, Bristol, BS8 1TD, UK

Abstract

Aims: Recurrent network activity in corticothalamic circuits generates physiological and pathological EEG waves. Many computer models have simulated spike-and-wave discharges (SWDs), the EEG hallmark of absence seizures (ASs). However, these models either provided detailed simulated activity only in a selected territory (i.e., cortical or thalamic) or did not test whether their corticothalamic networks could reproduce the physiological activities that are generated by these circuits.

Methods: Using a biophysical large-scale corticothalamic model that reproduces the full extent of EEG sleep waves, including sleep spindles, delta, and slow (<1 Hz) waves, here we investigated how single abnormalities in voltage- or transmitter-gated channels in the neocortex or thalamus led to SWDs.

Results: We found that a selective increase in the tonic γ-aminobutyric acid type A receptor (GABA-A) inhibition of first-order thalamocortical (TC) neurons or a selective decrease in cortical phasic GABA-A inhibition is sufficient to generate ~4 Hz SWDs (as in humans) that invariably start in neocortical territories. Decreasing the leak conductance of higher-order TC neurons leads to ~7 Hz SWDs (as in rodent models) while maintaining sleep spindles at 7–14 Hz.

Conclusion: By challenging key features of current mechanistic views, this simulated ictal corticothalamic activity provides novel understanding of ASs and makes key testable predictions.

KEYWORDS
cortex, GABA-A inhibition, GABA-B inhibition, thalamus, T-type Ca^{2+} channels

1 | INTRODUCTION

Absence seizures (ASs) are genetic, generalized, non-convulsive seizures characterized by sudden, relatively brief lapses of consciousness that are invariably accompanied by spike-and-waves discharges (SWDs) in the EEG.[1–5] It is well established that both the clinical and the electrographic symptoms of ASs originate from aberrant activity of corticothalamic networks[5] and a number of genetic abnormalities have been identified in humans with ASs.[6] However, our current understanding of how these genetic deficits lead to the ictal EEG activity observed during ASs is still not fully understood.

Many biophysical and non-biophysical models have simulated the generation of SWDs leading to increased knowledge of their underlying mechanisms.[7–21] However, these models either

provided detailed simulated activity only in a selected territory (i.e., cortical or thalamic) or did not test whether their corticothalamic networks could reproduce physiological activities that are known to be generated by these circuits.[22] Here, we used our corticothalamic model (Figure S1) that faithfully simulates EEG waves of natural sleep, that is, sleep spindles, delta, and slow (<1 Hz) waves[23] (Figure S2), to investigate whether single abnormal voltage- or transmitter-gated conductances bring about SWDs of ASs. In particular, we show that an increase in the tonic GABA-A inhibition of first-order thalamocortical (TC_{FO}) neurons, a decrease in cortical phasic GABA-A inhibition, an increase in cortical AMPA receptor function, or an increase in the T-type Ca^{2+} conductance of higher-order thalamocortical (TC_{HO}) neurons generates ~4 Hz SWDs (as observed in humans with ASs[2,5]) that invariably start in the neocortex.

2 | METHODS

2.1 | Corticothalamic network model

We used our biophysical model of the corticothalamic network (Figure S1) that faithfully reproduces the typical EEG waves of natural sleep (Figure S2).[23] Briefly, our corticothalamic model contains 900 model neurons and is organized into six sectors (Figure S1): four cortical layers, including layers 2/3 (L2/3), 4 (L4), 5 (L5), and 6 (L6), and a first- and a higher-order thalamic nucleus with their thalamocortical neurons (TC_{FO} and TC_{HO}, respectively) which are reciprocally connected to inhibitory NRT neurons (NRT_{FO} and NRT_{HO}, respectively).[24] Each cortical layer is divided into two subsectors, each with 100 excitatory and 50 inhibitory neurons. Cortical excitatory subsectors contain different numbers of regular spiking (RS), intrinsically bursting (IB), early firing (EF), repetitive intrinsically bursting (RIB), and network driver (ND) neurons, whereas inhibitory subsectors have FS interneurons (Figure S1). The full model is a two-dimensional stack of subsector neuron rows. The neuron position within a subsector was determined pseudo-randomly.[23]

2.2 | Model network connectivity

Connections were organized topographically with sources and targets located in matching regions of their corresponding structures. A neuron did not synapse onto itself and could only form a single synapse on its target neuron. The number of contacts that a source neuron could form in a target structure was defined by the parameter P (a projection radius). Other key connectivity parameters (e.g., connection weight, postsynaptic potential shape, synaptic transmission latency, and synaptic receptors) are described in detail in Dervinis and Crunelli.[23] Similarly, the numerical values of the various intrinsic and synaptic conductances of the different neuronal populations are detailed in Dervinis and Crunelli.[23]

2.3 | Simulations

All simulations were carried out in NEURON on a desktop computer or one of the following computing clusters: the Neuroscience Gateway (NSG) Portal for Computational Neuroscience or the Cardiff University School of Biosciences Biocomputing Hub HPC/Cloud infrastructure.

2.4 | Data analyses

Simulation data were analyzed and visualized with the help of custom-written Matlab (MathWorks Inc.) routines. The raw EEG signal was filtered and cross-correlated as described in Dervinis and Crunelli.[23] SWD Hilbert transform phase was calculated by band-pass filtering raw EEG traces using Butterworth filter with the following parameters: passband and stopband frequencies centered at ±2 Hz and ±4 Hz around the SWD oscillation frequency (~4 or ~7 Hz), respectively, and passband ripple and stopband attenuation being 0.5 and 65 dB, respectively. The filtered EEG signal was then subjected to Matlab's hilbert function. Hilbert phase synchronization index (PSI)[25] was calculated for two filtered signals obtained using the same filtering parameters as above and then smoothed using a moving average window of 1 s duration (for additional data analyses, see Appendix S1 in Dervinis and Crunelli[23]).

3 | RESULTS

As shown in the preceding paper,[23] our thalamocortical model is capable of smoothly transitioning between wakefulness (as evident from a low-amplitude, high-frequency EEG) and different EEG waves of natural sleep (depending on the input resistance of its constituent neurons) and it does not enter an overly synchronous activity-mode typical of seizures. However, one particular state of the model is prone to generate ictal states, that is, the transition between sleep and wakefulness. When the model is in this state, different single-membrane conductance changes in either cortical or thalamic neurons do lead to an EEG waveform typical of SWDs of ASs, as described below. Notably, all the changes in different conductances that lead to simulated SWDs have a minimal impact on sleep waves (not shown).

3.1 | Selective increase in tonic GABA-A inhibition of TC_{FO} neurons generates SWDs

Evidence in mouse and rat AS models have shown that an increased tonic GABA-A inhibition of TC_{FO} neurons (that results from higher thalamic GABA levels[26]) is necessary and sufficient for AS generation.[27–29] Moreover, higher levels of GABA were found in the thalamus of a child with ASs,[30] and drugs that are known to increase GABA levels, that is, vigabatrin and tiagabine, can induce

or aggravate ASs in humans.[31,32] Increasing (by 5%) the leak conductance (g_{KL}) in TC_{FO} neurons (in order to mimic the increased tonic GABA-A inhibition observed in genetic AS models[27,28]) led to the appearance of SWDs at ~4 Hz (Figure 1A$_1$,B$_1$; Table S1), a frequency similar to that in humans with ASs.[2,5] Further increases in g_{KL} did not change the SWD frequency and duration though decreased and then prolonged the interictal period (Figure 1A$_2$,A$_3$; Table S1).

At the single-cell level, almost all neuronal populations increased their total firing during SWDs except TC_{FO} neurons which showed a decrease (Figures 1B$_1$,B$_2$ and 2A). The same was observed for ictal burst firing, whereas tonic, single action potential (AP) firing decreased (Figure 2B,C). Indeed, burst firing was the highest contributor to ictal activity in all excitatory and inhibitory cortical neurons (independent from their layer location), but was absent in TC_{FO} neurons and similar to tonic firing in all NRT neurons (Figure 2D). Notably, all cortical and NRT neurons were never silent during SWDs, whereas both TC_{FO} and TC_{HO} neurons were mostly silent ictally or fired tonically (Figure 2D). When considering the firing dynamics of all ictal APs, all neuronal populations fired at or just after the SWD spike except TC_{FO} and TC_{HO} neurons that fired ~30 and 20 ms, respectively, prior to the SWD spike (Figure 2E$_1$,F$_1$). This is also reflected in the firing phase evolution throughout the SWD with TC_{FO} and TC_{HO} cells showing a positive phase through most of the SWD (leading) while cortical cells showing zero or slightly negative phase over the same period (lagging) (Figure 2G$_1$). However, when only the first AP of an SWD cycle was considered, all neurons fired ~10 ms before the SWD spike (Figure 2E$_2$), and almost all neuron types had a smaller peak ~80 ms prior to the SWD spike (Figure 2F$_2$). Notably, further increases in the tonic GABA-A inhibition of TC_{FO} neurons moved the peak of the first AP in each cycle to the left and the right in TC_{FO} and layer 4 pyramidal (L4/PY) neurons, respectively (Figure 2E$_3$,F$_3$). Spike-triggered action potential (STAP) histograms, however, do not decisively show which structures are leading during individual oscillation cycles. The temporal evolution of the phase of the first APs indicates that their phases do not remain stable (Figure 2G$_2$). Indeed, whereas the cortex is leading during the initial few seconds of the SWD (Figure 2G$_3$), the TC_{FO} cells briefly catch up and then gradually fall behind the cortical cells again (Figure 2G$_2$,G$_4$).

We then analyzed the temporal dynamics of firing synchrony within and between neuronal populations in the interictal and ictal periods (Figure 3). Within a given neural type, the stronger progressive increase in synchrony from interictal to ictal periods was observed in NRT_{FO} and NRT_{HO} neurons while the smallest increase occurred in TC_{FO} and TC_{HO} neurons (Figure 3A$_1$,$_2$). Among different populations, those involving all possible pairs of thalamic neurons showed the highest progressive synchrony as did the layer 5 pyramidal neurons (L5PY) pairs with either NRT or TC neurons, whereas the synchrony between L4PY and TC_{HO} neurons gradually decreased (Figure 3B$_3$). Thus, in summary, the temporal dynamics of increased

synchrony progress from thalamic and cortical neuron pairs to NRT neuron pairs and then to cortical and NRT neuron pairs (Figure 3C).

3.2 | SWD generation by other selective alterations in inhibitory and excitatory conductances

We first checked whether SWDs could be generated by an increase in conductance of the extrasynaptic GABA-A receptors (g_{eGABAa}) of TC_{FO} neurons instead of indirectly increasing the g_{KL} of these neurons. As shown in Figure 4B$_{1-4}$, progressive enhancement of this conductance reliably elicited SWDs. Moreover, selectively decreasing (by 10% and 25%) the conductance of the phasic GABA-A inhibition (g_{GABAa}) in all cortical neurons led to SWDs (as observed in vivo experiments[33-36]) of progressively larger amplitude and increasingly longer interictal periods (Figure 4C$_{1-3}$; Table S2). Compared to the SWDs generated by an increase in thalamic tonic GABA-A inhibition, stronger synchrony was observed between L5PY and all NRT neuron pairs as well as between L4PY and TC_{HO} neuron pairs in the simulated activity induced by a decreased cortical g_{GABAa} (Figure 4C$_4$).

Progressively increasing (by 5% and 40%) the conductance of cortical AMPA receptors (g_{AMPA}) also led to more frequent SWDs of increasing amplitude (Figure 4D$_{1,3}$) (Table S2) and lower synchrony between L5PY and NRT neurons, compared to SWDs elicited by decreased cortical g_{GABAa} (Figure 4D$_4$).

A higher number of cortical strongly intrinsically bursting (SIB) neurons have been reported in genetic rat models of ASs[37,38]: its implementation in the model indeed generated SWDs although of a small amplitude compared to changes in other conductances (Figure 4E$_{1-3}$; Table S2) and with a characteristic interictal-to-ictal decrease in synchrony in L4PY-TC_{HO}, L5PY-TC_{HO}, NRT_{HO}-TC_{FO}, and NRT_{HO}-TC_{HO} neuron pairs (Figure 4E$_4$).

Finally, increasing the conductance of the T-type Ca^{2+} channels (g_T) in all NRT neurons, as it has been observed in both humans and experimental models of ASs,[39,40] led to brief, small-amplitude SWDs, which, notably, were abolished by a further increase in this conductance (Figure 4F$_{1-4}$). Moreover increasing (by 5% and 10%) g_T in TC_{HO} neurons (Table S2) generated progressively longer SWDs, ultimately leading to absence status (Figure 4G$_{1,3}$), and a gradual increase in synchrony among almost all neuronal pairs (Figure 4G$_4$).

3.3 | Critical conductances of simulated SWDs

Having established that our model reproduces SWDs elicited by either increasing thalamic tonic or decreasing cortical phasic GABA-A inhibition, we next studied which effect other conductances have on these simulated SWDs. Removing g_T from TC_{FO} neurons did not abolish SWDs, as recently reported,[41] but actually increased their amplitude and decreased the interictal period duration (Figure 5B$_{1,2}$). In contrast, removing g_T from TC_{HO} neurons abolished SWDs elicited by both increased thalamic tonic and decreased cortical phasic

FIGURE 1   Selective increase in tonic GABA-A inhibition of TC_{FO} neurons elicits SWDs. (A_1) EEG traces show the induction of spontaneous SWDs at ~4Hz after progressive increases in g_{KL} of TC_{FO} neurons, mimicking the constitutively high tonic GABA-A inhibition reported in AS models. The control condition shows simulated desynchronized state typical of relaxed wakefulness. The SWD in the shaded area is expanded in B_1. (A_2) Cross-correlations between APs of all neurons and the EEG calculated over a 20min simulation period. Shaded regions represent 95% confidence intervals. (A_3) Schematic timeline showing ictal and interictal periods for different g_{KL} values. Color code as in (A_2). (B_1) Top trace: EEG. Panels below show the membrane potential (upper trace) of the indicated neuron and a color-coded graph of the membrane potential of all neurons of the indicated population. Red bars on the membrane potential traces indicate −60mV. Red arrowheads in the color-coded graphs mark the neuron shown in the corresponding membrane potential trace. (B_2) Same as (B_1), shows the expanded SWD cycle highlighted in (B1). Vertical red dotted line marks the peak of the SWD spike. L4 PY, Pyramidal neuron in cortical layer 4; L5 PY, pyramidal neuron in cortical layer 5; L5 IN, interneuron in cortical layer 5; TC_{FO}, first-order TC neuron; TC_{HO}, higher-order TC neuron; NRT_{FO}, first-order NRT neuron; NRT_{HO}, higher-order NRT neuron.

GABA-A inhibition (Figure $5C_{1,2}$) as did g_T removal from all types of NRT neurons (Figure $5D_{1,2}$).

Blocking the conductances of GABA-B receptors (g_{GABAb}) in either all cortical or thalamic neurons abolished SWDs generated by increased thalamic tonic and decreased cortical phasic GABA-A inhibition (Figure $5E_{1,2},F_{1,2},G_{1,2}$) as shown experimentally.[42–45] In contrast, increasing g_{GABAb} in cortical neurons decreased the amplitude of SWDs and markedly increased their duration (Figure $5H_{1,2}$). Enhancing g_{GABAb} in TC_{FO} neurons increased the amplitude and the interictal period of SWDs elicited by the increased thalamic tonic GABA-A inhibition (Figure $5I_1$), whereas it decreased the interictal period of the SWDs simulated by a decreased cortical phasic GABA-A inhibition (Figure $5I_2$). Finally, increasing g_{GABAb} in TC_{HO} neurons led to absence status in both models (Figure $5J_{1,2}$).

Next, we investigated which conductance was critical for determining the simulated intra-SWD frequency as it represents a major difference between ASs in human and animal models. We found that both in the models with an increased thalamic tonic and decreased cortical phasic GABA-A inhibition, a reduction of the g_{KL} of TC_{HO} neurons increased the frequency of SWDs from ~4Hz to the 7–8Hz (compare Figure $6A_{1,2}$ with $D_{1,2}$), a value that is typical of mouse and rat genetic and pharmacological models.[1,3–5]

Finally, since the non-selective cation conductance (g_{CAN}) plays a key role in some EEG waves of natural[46–48] and simulated[23] sleep and its involvement in ASs has not been studied before, we investigated whether it is necessary for simulated SWDs. Removing g_{CAN} from all TC neurons had little effect on SWDs (Figure $6G_{1,2}$). In contrast, removal of (g_{CAN}) from all NRT neurons led to absence status in the model with increased g_{KL} of TC_{FO} neurons (Figure $6H_1$) and markedly prolonged SWDs in the model with decreased g_{GABAa} in cortical neurons (Figure $6H_2$).

4 | DISCUSSION

The main finding of this study is the ability to faithfully reproduce SWDs at the 4Hz frequency observed in human ASs by single modifications of neocortical or thalamic conductances in a corticothalamic model that faithfully reproduces the intrinsic and network activity observed in neocortical and thalamic territories during natural sleep.[23] To the best of our knowledge, this is the most detailed

large-scale model dedicated to simulating SWDs, and its component parts and their connectivity patterns were replicated with a high degree of fidelity to experimental data.[22] Constructing a multipurpose model guards against an implementation bias of favoring a particular (patho)physiological regime. In fact, no previous attempt at modeling SWDs had this level of physiological validity.

4.1 | Model limitations

Notwithstanding, our model has a number of limitations (see Dervinis and Crunelli[23] for details). In the absence of direct measurements, the T-type Ca^{2+} current implemented in various types of neocortical neurons was guided by the ability of these neurons to faithfully reproduce intrinsic slow (<1Hz) waves.[23] Moreover, although no detailed parameters exist for the persistent Na^+ current in NRT neurons, this current (with biophysical properties similar to those reported for TC neurons[46]) had to be introduced in NRT neurons in order to faithfully reproduce the intrinsic slow (<1Hz) waves observed in in vitro studies.[48] Finally, since no voltage-clamp study has been performed in higher-order thalamic nuclei, the biophysical properties of the conductances of TC_{HO} neurons were inferred from current-clamp data and/or adapted from TC_{FO} neurons.[49–52]

4.2 | Simulation strength

The solidity of our simulated SWDs is supported by two major findings. First, our model faithfully reproduces the three main EEG waves generated by corticothalamic networks during sleep, that is, spindle, delta, and slow (<1Hz) waves,[23] and these natural rhythms are only minimally affected by the different changes in single voltage- and transmitter-gated conductances that lead to SWDs. Second, our model is capable of reproducing many experimental findings after implementing the different abnormalities that are known to be present in humans with, and genetic models of, ASs.

In particular, our model generates ~4Hz SWDs following:

1. blockade of neocortical phasic GABA-A inhibition, as shown experimentally following intracortical injection of the weak and potent GABA-A antagonists penicillin and bicuculline, respectively[33–36,53–55];
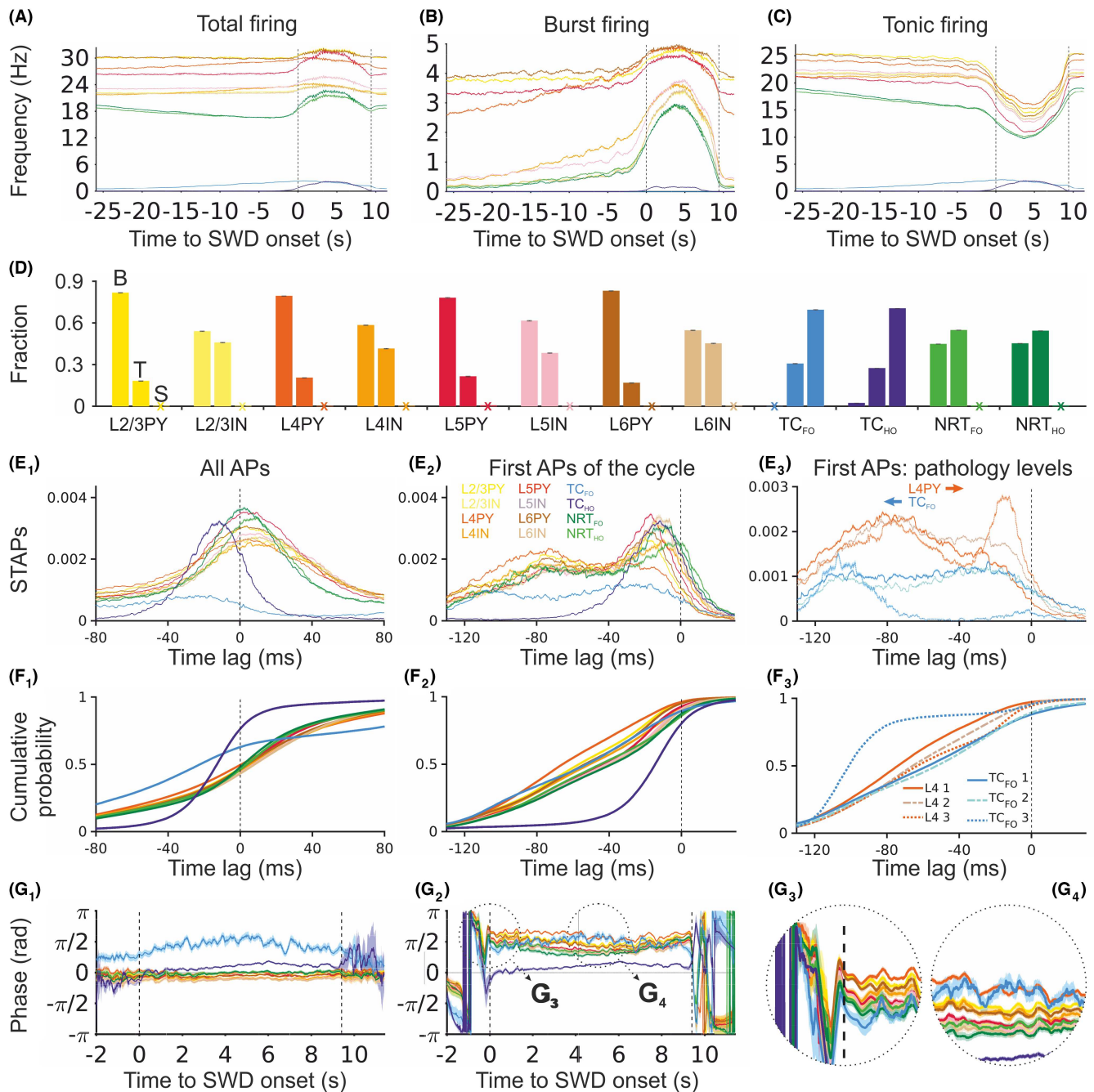
FIGURE 2 Firing properties during SWDs elicited by increased tonic GABA-A inhibition of TC_{FO} neurons. (A–C) Interictal and ictal time evolution of total, burst, and tonic firing frequency for the indicated neuron types. Ictal and interictal periods were linearly scaled to their average durations. The shaded regions represent 95% confidence intervals. Dashed vertical black lines represent the onset and offset of the averaged SWD. Color-code as in (E_2). (D) Mean proportion of the indicated neurons showing burst and tonic firing (B and T column, respectively) and those that are silent (S column). Error bars indicate 95% confidence intervals. (E_1) Cross-correlations between all APs of different neuronal types and the SWD spike (SWD spike-triggered action potentials: STAPs). Shaded regions are 95% confidence intervals. Dashed vertical line indicates the peak of the SWD spike. Color-code as in (E_2). (E_2) Same as (E_1) but only for the first AP in an SWD cycle. (E_3) Same as (E_2) but only for L4PY and TC_{FO} neurons for the three color-coded g_{KL} values indicated in (F_3) and Figure 1A_2. Arrows indicate the shift of the firing peaks as g_{KL} is increased. (F_{1-3}) Cumulative AP probability corresponding to (E_{1-3}). (G_1) Hilbert transform mean phase of APs of all cell types with respect to the SWD spike. Different SWDs were linearly scaled to the average duration SWD. Dashed vertical lines indicate the SWD onset and offset. Shaded regions represent 95% confidence intervals. Color code as in (E_2). (G_2) Same as (G_1) but only for the first AP in an SWD cycle. ($G_{3,4}$) Same as (G_2) showing the enlarged regions circled in (G_2). L2/3 PY, pyramidal neuron in cortical layers 2 and 3; L2/3 IN, interneuron in cortical layers 2 and 3; L4 PY, pyramidal neuron in cortical layer 4; L4 IN, interneuron in cortical layer 4; L5 PY, pyramidal neuron in cortical layer 5; L5 IN, interneuron in cortical layer 5; L6 PY, pyramidal neuron in cortical layer 6; L6 IN, interneuron in cortical layer 6; TC_{FO}, first-order TC neuron; TC_{HO}, higher-order TC neuron; NRT_{FO}, first-order NRT neuron; NRT_{HO}, higher-order NRT neuron.

2. increase in the tonic GABA-A inhibition of TC_{FO} neurons, by directly increasing the function of extrasynaptic GABA-A receptors or indirectly increasing the g_{KL} of these neurons, as shown in different genetic models of ASs,[27] that is, the GAERS (Genetic Absence Epilepsy Rats from Strasbourg) rats and the stargazer and lethargic mouse models;

3. enhancement of GABA-B inhibition in either thalamic or cortical territory, as shown by the generation and aggravation of SWDs in normal mice and rats and genetic AS models, respectively, following systemic, intracortical, and intrathalamic injection of GABA-B receptor agonists[42–45];
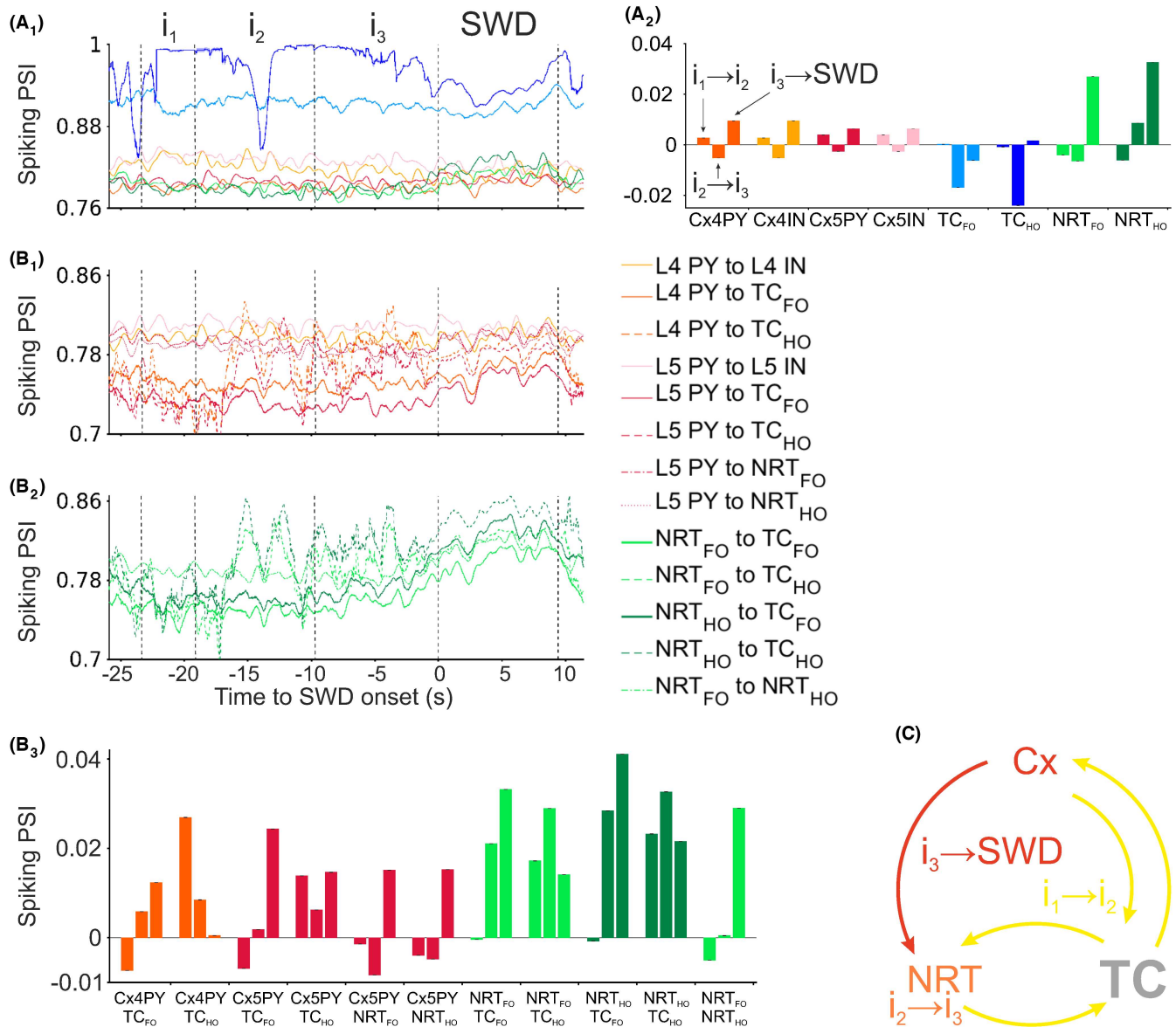

FIGURE 3 Time evolution of interictal and ictal firing synchrony for SWDs elicited by increased tonic GABA-A inhibition of TC_{FO} neurons. (A₁) Ictal and interictal mean phase synchronization index (PSI) of APs within a neuronal population (color-code as in Figure 2E₂). Ictal and interictal periods were linearly scaled to their average durations. Dashed vertical black lines indicate different parts of ictal and interictal periods: i_1 marks a section from 1/6 to 1/3 of the interictal period, i_2 marks the 1/3 to 2/3 section, i_3 marks the final third of the interictal period, and the last two lines indicate the start and end of the ictal period. (A₂) Changes in PSI during interictal and ictal periods. For each indicated neuronal population, the left bar is the PSI change between i_1 and i_2 ($i_1 \rightarrow i_2$), the middle bar between i_2 and i_3 ($i_2 \rightarrow i_3$), and the right bar between i_3 and the ictal period ($i_3 \rightarrow$ SWD). (B₁,₂) Evolution of ictal and interictal PSI between different cortical (B₁) and thalamic (B₂) populations (color-code on the right). Vertical dashed black lines demarcate the same regions as in (A₁). (B₃) Changes in PSI of different neuronal populations over interictal and ictal periods. For each neuronal population pair, the three bars are as in (A₂). (C) Schematic representation of the evolution of PSI. Brian areas and their connections shaded in yellow show increase in PSIs between i_1 and i_2 and represent the initial synchronization stage (corresponding to bar 1 in all comparison groups of A₂ and B₃). Orange and red colors mark PSI increases during the second synchronization stage (between i_2 and i_3) and the final synchronization stage (between i_3 and the ictal period), respectively.
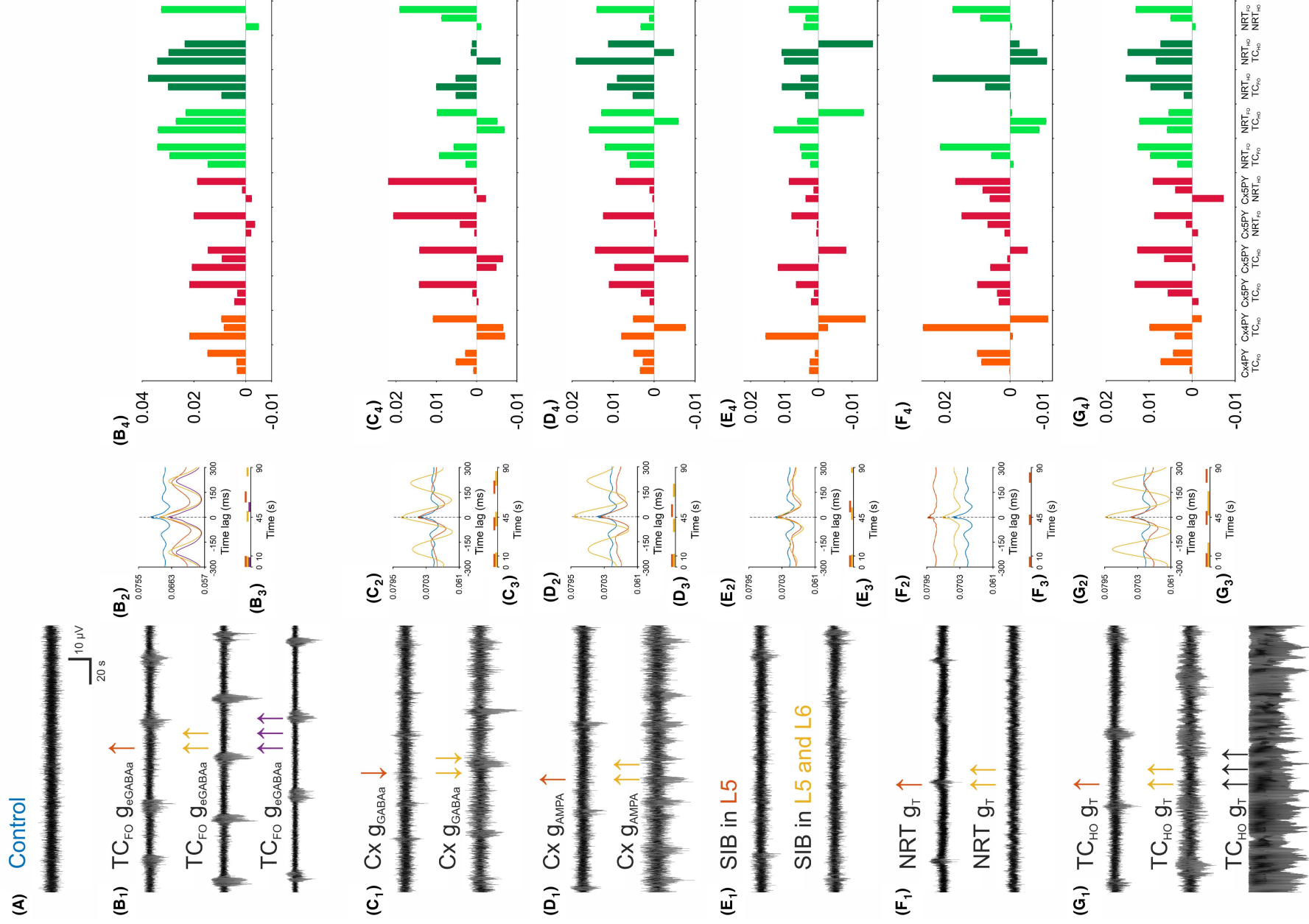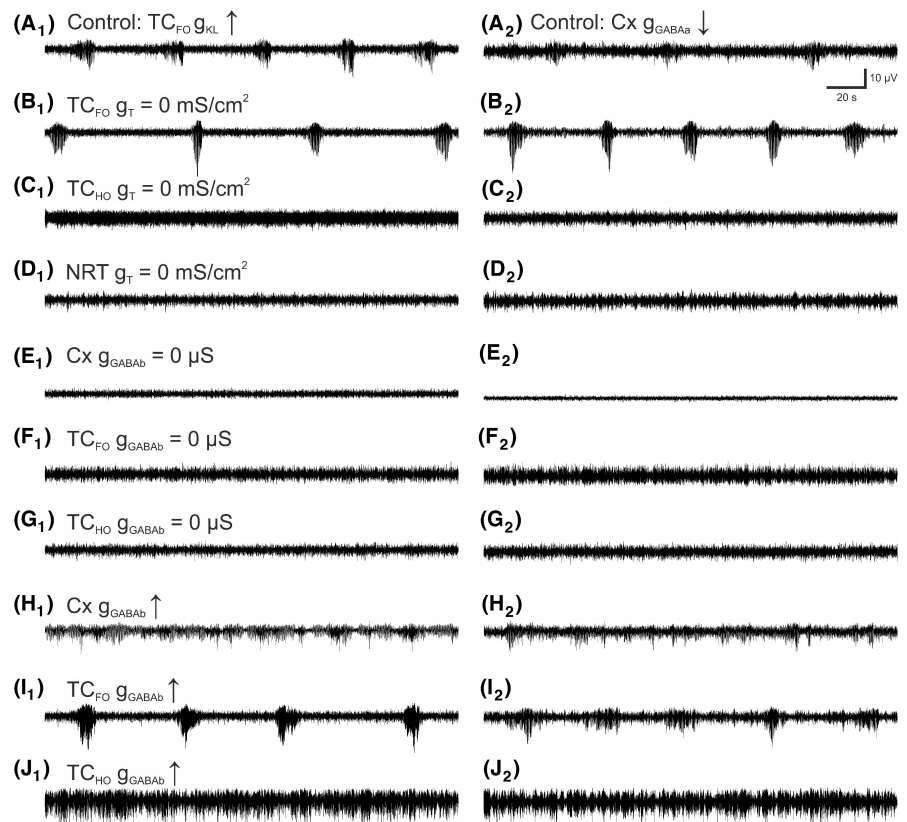
FIGURE 4 Thalamic and cortical abnormalities can independently induce SWDs. (A) EEG showing a period of simulated desynchronized state. (B_1) SWDs elicited by progressive increases in the extrasynaptic GABA-A conductance (g_{eGABAa}) of TC_{FO} neurons. (B_2) Cross-correlations between APs of all cells and EEG (over a 20 min simulation period) with increased TC_{FO} neuron g_{eGABAa}. Color code as in B1. Shaded regions represent 95% confidence intervals. (B_3) Schematic SWD timeline showing SWD duration and frequency of occurrence for different TC_{FO} neuron g_{eGABAa} levels. (B_4) Change in the firing PSI between the indicated neuronal populations in (G_4). For each neuronal population pair, the left bar is the PSI change between i_1 and i_2 ($i_1 \rightarrow i_2$), the middle bar between i_2 and i_3 ($i_2 \rightarrow i_3$), and the right bar between i_3 and the ictal period ($i_3 \rightarrow$ SWD), as indicated in Figure 3A$_2$. (C_{1-4}) same as (B_{1-4}) but showing SWDs following decreases in GABA-A conductance (g_{GABAa}) of all cortical neurons. (D_{1-4}) same as (B_{1-4}) but showing SWDs following increases in the cortical AMPA receptor conductance (g_{AMPA}). (E_{1-4}) same as (B_{1-4}) but showing SWDs elicited by the addition of strongly intrinsically bursting (SIB) neurons in cortical layer 5 (L5) only or in both L5 and cortical layer 6 (L6). (F_{1-4}) same as (B_{1-4}) but showing SWDs after increases in the T-type Ca^{2+} conductance (g_T) of NRT cells. (G_{1-4}) same as (B_{1-4}) but showing SWDs after increases in the T-type Ca^{2+} conductance (g_T) of TC_{HO} cells. Note the absence status reached the highest increase of g_T in these thalamic neurons.

FIGURE 5 Essential contribution of various voltage- and transmitter-gated conductances to simulated SWDs. (A_1) Control SWDs elicited by increased g_{KL} in TC_{FO} neurons. (A_2) Control SWDs elicited by decreased neocortical g_{GABAa}. ($B_{1,2}$) SWDs persist after blocking g_T in TC_{FO} neurons. ($C_{1,2}$) SWDs are not generated when g_T is blocked in TC_{HO} neurons. ($D_{1,2}$) SWDs are not elicited when g_T is blocked in all NRT neurons. ($E_{1,2}$) SWDs are blocked after removing g_{GABAb} in all neocortical neurons. ($F_{1,2}$) SWDs are blocked after removing g_{GABAb} in TC_{FO} neurons. ($G_{1,2}$) SWDs are blocked after removing g_{GABAb} in TC_{HO} neurons. ($H_{1,2}$) Smaller-amplitude, almost continuous SWDs are elicited when g_{GABAb} is increased in neocortical neurons. ($I_{1,2}$) the SWD amplitude and the interictal period are increased when g_{GABAb} is increased in TC_{FO} neurons. ($J_{1,2}$) Absence status is generated when g_{GABAb} is increased in TC_{HO} neurons.

(A_1) Control: TC_{FO} g_{KL} ↑   (A_2) Control: Cx g_{GABAa} ↓
(B_1) TC_{FO} g_T = 0 mS/cm^2 (B_2)
(C_1) TC_{HO} g_T = 0 mS/cm^2 (C_2)
(D_1) NRT g_T = 0 mS/cm^2 (D_2)
(E_1) Cx g_{GABAb} = 0 µS   (E_2)
(F_1) TC_{FO} g_{GABAb} = 0 µS   (F_2)
(G_1) TC_{HO} g_{GABAb} = 0 µS   (G_2)
(H_1) Cx g_{GABAb} ↑   (H_2)
(I_1) TC_{FO} g_{GABAb} ↑   (I_2)
(J_1) TC_{HO} g_{GABAb} ↑   (J_2)

10 µV
20 s

4. increase in the T-type Ca^{2+} channel function in TC_{HO} neurons, as reported by Gorji et al.[49] and Seidenbecher et al.[50];

5. increase in the T-type Ca^{2+} channel function in NRT neurons, as reported by Chen et al.[39] and Cain et al.[40]; and

6. enhancement of the number of intrinsically bursting cells in layers 5/6, as observed in the Wistar Albino Glaxo Rats from Rijswijk[37] and the GAERS genetic models of ASs.[38]

Our simulations also show that SWDs are abolished or reduced following (1) blockade of cortical or thalamic GABA-B receptors as observed in different genetic and pharmacological models of ASs following systemic, intracortical, or intrathalamic injection of selective GABA-B receptor antagonists[40–43]; and (2) removal of T-type Ca^{2+} channels in NRT neurons, as seen following intra-NRT infusion of TTA-P2,[39] a potent and selective blocker of these channels,[56] in

GAERS rats. In contrast, simulated SWDs are unaffected by blocking T-type Ca^{2+} channels in TC_{FO} neurons as reported by McCafferty et al.[41] Notably, an increase in g_T of all NRT neurons, as observed in humans and models of ASs,[39,40] only led to brief, small-amplitude SWDs, clearly indicating that this thalamic abnormality is not capable alone to induce a solid absence phenotype.

Finally, the strength of our results is also supported by their similarities with the following experimental findings:

1. TC_{FO} neurons, as those in the ventrobasal thalamus, are mostly silent during SWDs[41,57];

2. burst firing of NRT and cortical neurons increases during SWDs[41,58];

3. tonic firing is reduced in all types of cells, as shown experimentally,[41] except in TC_{HO} cells for which no data are available at present;
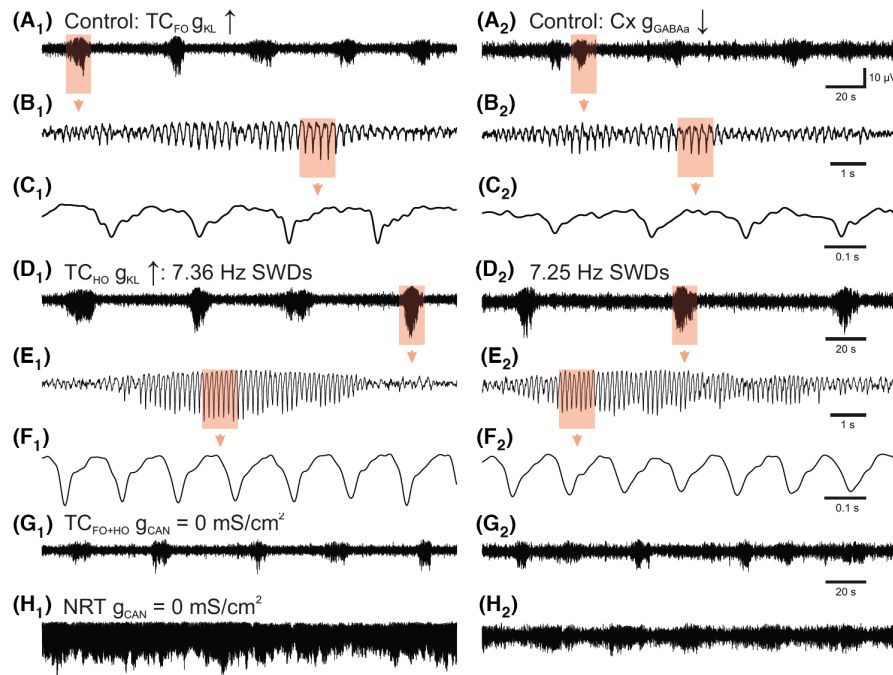
FIGURE 6 Effect of I_{CAN} and control of SWD frequency by g_{KL} of TC_{HO} neurons. (A_1) Control SWDs elicited by increased g_{KL} in TC_{FO} neurons. (A_2) Control SWDs elicited by decreased neocortical g_{GABAa}. Highlighted areas are enlarged below the corresponding traces (B and C). ($D_{1,2}$) Decreasing g_{KL} in TC_{HO} neurons leads to SWDs at ~7 Hz (typical of AS models) in both the model with increased g_{KL} of TC_{FO} neurons and that with decreased g_{GABAa} in cortical neurons. Highlighted areas are enlarged below the corresponding traces (E and F). ($G_{1,2}$) Blocking g_{CAN} in TC_{FO} and TC_{HO} neurons has very little effect on the SWDs generated by both models. (H_1) Blocking g_{CAN} in all NRT neurons transforms the well-separated SWDs elicited by the increased g_{KL} in TC_{FO} neurons into absence status. (H_2) Blocking g_{CAN} in all NRT neurons of the model with decreased g_{GABAa} in cortical neurons markedly prolongs the duration of SWDs.

4. the burst firing of cortical pyramidal neurons and interneurons in all layers is increased ictally compared to interical periods[38,41,59];

5. the transition between sleep and quiet wakefulness is the vigilance state where most SWDs occur.[60,61]

4.3 | Predictions from simulated SWDs

A number of key testable predictions originate from the results of our study:

1. T-type Ca^{2+} channel-mediated burst firing in TC_{HO} neurons is necessary to elicit SWDs;

2. depolarization of TC_{FO} neurons prevents SWD generation or interferes with ongoing SWDs;

3. I_{CAN} of NRT neurons is essential for termination of SWDs;

4. g_{KL} of TC_{HO} neurons is a key determinant of SWD frequency;

5. absence status occurs when (i) blocking I_{CAN} in NRT neurons, (ii) strongly increasing g_T in TC_{HO} neurons, and (iii) increasing g_{GABAb} in TC_{HO} neurons. These results provide the first mechanistic insight into absence status and have a strong translational significance since both T-type Ca^{2+} channel blockers and GABA-B receptor antagonists are being trialed in human cohorts.[5]

CONFLICT OF INTEREST STATEMENT

The authors declare no conflict of interest.

DATA AVAILABILITY STATEMENT

The model codes are available to download from Github via Zenodo (https://doi.org/10.5281/zenodo.7724411 and https://doi.org/10.5281/zenodo.7724443).

ORCID

Vincenzo Crunelli https://orcid.org/0000-0001-7154-9752

REFERENCES

1. Crunelli V, Leresche N. Childhood absence epilepsy: genes, channels, neurons and networks. *Nat Rev Neurosci*. 2002;3:371-382.
2. Blumenfeld H. Cellular and network mechanisms of spike-wave seizures. *Epilepsia*. 2005;46(Suppl 9):21-33.
3. Scheffer IE, Berg AT. Classification and clinical features of absence epilepsies: how evidence leads to changing concepts. *Epilepsia*. 2008;49:2140-2141.

4. Meeren H, van Luijtelaar G, Lopes da Silva F, Coenen A. Evolving concepts on the pathophysiology of absence seizures: the cortical focus theory. *Arch Neurol*. 2005;62:371-376.

5. Crunelli V, Lőrincz ML, McCafferty C, et al. Clinical and experimental insight into pathophysiology, comorbidity and therapy of absence seizures. *Brain*. 2020;143:2341-2368.

6. International League Against Epilepsy Consortium on Complex Epilepsies. Genome-wide mega-analysis identifies 16 loci and highlights diverse biological mechanisms in the common epilepsies. *Nat Commun*. 2018;9:5269.

7. Bazhenov M, Timofeev I, Steriade M, Sejnowski TJ. Model of thalamocortical slow-wave sleep oscillations and transitions to activated states. *J Neurosci*. 2002;22:8691-8704.

8. Destexhe A. Spike-and-wave oscillations based on the properties of GABAB receptors. *J Neurosci*. 1998;18:9099-9111.

9. Destexhe A. Can GABAA conductances explain the fast oscillation frequency of absence seizures in rodents? *Eur J Neurosci*. 1999;11:2175-2181.

10. Medvedeva TM, Sysoeva MV, van Luijtelaar G, Sysoev IV. Modeling spike-wave discharges by a complex network of neuronal oscillators. *Neural Netw*. 2018;98:271-282.

11. Lytton WW, Contreras D, Destexhe A, Steriade M. Dynamic interactions determine partial thalamic quiescence in a computer network model of spike-and-wave seizures. *J Neurophysiol*. 1997;77:1679-1696.

12. Destexhe A, Bal T, McCormick DA, Sejnowski TJ. Ionic mechanisms underlying synchronized oscillations and propagating waves in a model of ferret thalamic slices. *J Neurophysiol*. 1996;76:2049-2070.

13. Wang XJ, Gloomy D, Rinzel J. Emergent spindle oscillations and intermittent burst firing in a thalamic model: specific neuronal mechanisms. *Proc Natl Acad Sci U S A*. 1995;92:5577-5581.

14. Marten F, Rodrigues S, Benjamin O, Richardson M, Terry J. Onset of polyspike complexes in a mean-field model of human electroencephalography and its application to absence epilepsy. *Philos Trans A Math Phys Eng Sci*. 2009;367:1145-1161.

15. Taylor P, Thomas J, Sinha N, et al. Optimal control based seizure abatement using patient derived connectivity. *Front Neurosci*. 2015;9:202.

16. Schmidt H, Petkov G, Richardson M, Terry L. Dynamics on networks: the role of local dynamics and global networks on the emergence of hypersynchronous neural activity. *PLoS Comp Biol*. 2014;10:e1003947.

17. Destexhe A. Network models of absence seizures. In: Faingold CL, Blumenfeld H, eds. *Neuronal Networks in Brain Function, CNS Disorders, and Therapeutics*. Elsevier; 2014:11-35.

18. Yang DP, Robinson PA. Unified analysis of global and focal aspects of absence epilepsy via neural field theory of the corticothalamic system. *Phys Rev E*. 2019;100:032405.

19. Breakspear M, Roberts JA, Terry JR, Rodrigues S, Mahant N, Robinson PA. A unifying explanation of primary generalized seizures through nonlinear brain modeling and bifurcation analysis. *Cereb Cortex*. 2006;16:1296-1313.

20. Medvedeva TM, Sysoeva MV, Lüttjohann A, van Luijtelaar G, Sysoev IV. Dynamical mesoscale model of absence seizures in genetic models. *PLoS One*. 2020;15:e0239125.

21. Fan D, Liu S, Wang Q. Stimulus-induced epileptic spike-wave discharges in Thalamocortical model with disinhibition. *Sci Rep*. 2016;6:37703.

22. Lorincz ML, Gunner D, Bao Y, et al. A distinct class of slow (~0.2–2 Hz) intrinsically bursting layer 5 pyramidal neurons determines UP/DOWN state dynamics in the neocortex. *J Neurosci*. 2015;35:5442-5458.

23. Dervinis M, Crunelli V. Sleep waves in a large-scale corticothalamic model constraint by cortical and thalamic single neuron- and network-intrinsic activities. *CNS Ther & Neurosci*. 2023. doi:10.1101/2022.10.31.514504

24. Sherman SM. Thalamic relays and cortical functioning. *Prog Brain Res*. 2005;149:107-126.

25. Quian Quiroga R, Kraskov A, Kreuz T, Grassberger P. Performance of different synchronization measures in real data: a case study on electroencephalographic signals. *Phys Rev E*. 2002;65:041903.

26. Richards DA, Lemos T, Whitton PS, Bowery NG. Extracellular GABA in the ventrolateral thalamus of rats exhibiting spontaneous absence epilepsy: a microdialysis study. *J Neurochem*. 1995;65:1674-1680.

27. Cope DW, Di Giovanni G, Fyson SJ, et al. Enhanced tonic GABAA inhibition in typical absence epilepsy. *Nat Med*. 2009;15:1392-1398.

28. Errington AC, Gibson KM, Crunelli V, Cope DW. Aberrant GABA(a) receptor-mediated inhibition in cortico-thalamic networks of succinic semialdehyde dehydrogenase deficient mice. *PLoS One*. 2011;6:e19021.

29. Crunelli V, Cope DW, Terry JR. Transition to absence seizures and the role of GABA(a) receptors. *Epilepsy Res*. 2011;97:283-289.

30. Leal A, Vieira JP, Lopes R, et al. Dynamics of epileptic activity in a peculiar case of childhood absence epilepsy and correlation with thalamic levels of GABA. *Epilepsy Behav Case Rep*. 2016;5:57-65.

31. Perucca E, Gram L, Avanzini G, Dulac O. Antiepileptic drugs as a cause of worsening seizures. *Epilepsia*. 1998;39:5-17.

32. Ettinger AB, Bernal OG, Andriola MR, et al. Two cases of nonconvulsive status epilepticus in association with tiagabine therapy. *Epilepsia*. 1999;40:1159-1162.

33. Steriade M, Contreras D. Spike-wave complexes and fast components of cortically generated seizures. I. Role of neocortex and thalamus. *J Neurophysiol*. 1998;80:1439-1455.

34. Avoli M, Gloor P. Interaction of cortex and thalamus in spike and wave discharges of feline generalized penicillin epilepsy. *Exp Neurol*. 1982;76:196-217.

35. Luhmann HJ, Mittmann T, van Luijtelaar G, Heinemann U. Impairment of intracortical GABAergic inhibition in a rat model of absence epilepsy. *Epilepsy Res*. 1995;22:43-51.

36. D'Antuono M, Inaba Y, Biagini G, D'Arcangelo G, Tancredi V, Avoli M. Synaptic hyperexcitability of deep layer neocortical cells in a genetic model of absence seizures. *Genes Brain Behav*. 2006;5:73-84.

37. Kole MH, Brauer AU, Stuart GJ. Inherited cortical HCN1 channel loss amplifies dendritic calcium electrogenesis and burst firing in a rat absence epilepsy model. *J Physiol*. 2007;578:507-525.

38. Polack PO, Guillemain I, Hu E, Deransart C, Depaulis A, Charpier S. Deep layer somatosensory cortical neurons initiate spike-and-wave discharges in a genetic model of absence seizures. *J Neurosci*. 2007;27:6590-6599.

39. Chen Y, Lu J, Pan H, et al. Association between genetic variation of *CACNA1H* and childhood absence epilepsy. *Ann Neurol*. 2003;54:239-243.

40. Cain SM, Tyson JR, Choi H, et al. CaV3.2 drives sustained burst-firing, which is critical for absence seizure propagation in reticular thalamic neurons. *Epilepsia*. 2018;59:778-791.

41. McCafferty C, David F, Venzi M, et al. Cortical drive and thalamic feed-forward inhibition control thalamic output synchrony during absence seizures. *Nat Neurosci*. 2018;21:744-756.

42. Hosford DA, Clark S, Cao Z, et al. The role of GABAB receptor activation in absence seizures of lethargic (lh/lh) mice. *Science*. 1992;257:398-401.

43. Liu Z, Vergnes M, Depaulis A, Marescaux C. Involvement of intrathalamic GABAb neurotransmission in the control of absence seizures in the rat. *Neuroscience*. 1992;48:87-93.

44. Liu Z, Vergnes M, Depaulis A, Marescaux C. Evidence for a critical role of GABAergic transmission within the thalamus in the genesis and control of absence seizures in the rat. *Brain Res*. 1991;545:1-7.

45. Charpier S, Leresche N, Deniau JM, Mahon S, Hughes SW, Crunelli V. On the putative contribution of GABA(B) receptors to the electrical events occurring during spontaneous spike and wave discharges. *Neuropharmacology.* 1999;38:1699-1706.

46. Hughes SW, Cope DW, Blethyn KL, Crunelli V. Cellular mechanisms of the slow (<1 Hz) oscillation in thalamocortical neurons in vitro. *Neuron.* 2002;33:947-958.

47. Crunelli V, Hughes SW. The slow (<1 Hz) rhythm of non-REM sleep: a dialogue between three cardinal oscillators. *Nat Neurosci.* 2010;13:9-17.

48. Blethyn KL, Hughes SW, Tóth TI, Cope DW, Crunelli V. Neuronal basis of the slow (<1 Hz) oscillation in neurons of the nucleus Reticularis thalami In vitro. *J Neurosci.* 2006;26:2474-2486.

49. Gorji A, Mittag C, Shahabi P, Seidenbecher T, Pape HC. Seizure-related activity of intralaminar thalamic neurons in a genetic model of absence epilepsy. *Neurobiol Dis.* 2011;43:266-274.

50. Seidenbecher T, Pape HC. Contribution of intralaminar thalamic nuclei to spike-and-wave-discharges during spontaneous seizures in a genetic rat model of absence epilepsy. *Eur J Neurosci.* 2001;13:1537-1546.

51. Destexhe A, Contreras D, Steriade M, Sejnowski TJ, Huguenard JR. In vivo, in vitro, and computational analysis of dendritic calcium currents in thalamic reticular neurons. *J Neurosci.* 1996;16:169-185.

52. Connelly WM, Crunelli V, Errington AC. Variable action potential backpropagation during tonic firing and low-threshold spike bursts in thalamocortical but not thalamic reticular nucleus neurons. *J Neurosci.* 2017;37:5319-5333.

53. Crunelli V, Leresche N, Cope DW. GABA-A receptor function in typical absence seizures. In: Noebels JL, Avoli M, Rogawski MA, Olsen RW, Delgado-Escueta AV, eds. *Jasper's Basic Mechanisms of the Epilepsies.* 4th ed. National Center for Biotechnology Information (US); 2012.

54. Fisher RS, Prince DA. Spike-wave rhythms in cat cortex induced by parenteral penicillin. I. Electroencephalographic features. *Electroencephalogr Clin Neurophysiol.* 1977;42:608-624.

55. Gloor P, Quesney LF, Zumstein H. Pathophysiology of generalized penicillin epilepsy in the cat: the role of cortical and subcortical structures. II. Topical application of penicillin to the cerebral cortex and to subcortical structures. *Electroencephalogr Clin Neurophysiol.* 1977;43:79-94.

56. Dreyfus FM, Tscherter A, Errington AC, et al. Selective T-type calcium channel block in thalamic neurons reveals channel redundancy and physiological impact of I(T)window. *J Neurosci.* 2010;30:99-109.

57. Pinault D, Leresche N, Charpier S, et al. Intracellular recordings in thalamic neurones during spontaneous spike and wave discharges in rats with absence epilepsy. *J Physiol.* 1998;509:449-456.

58. Slaght SJ, Leresche N, Deniau JM, Crunelli V, Charpier S. Activity of thalamic reticular neurons during spontaneous genetically determined spike and wave discharges. *J Neurosci.* 2002;22:2323-2334.

59. Chipaux M, Charpier S, Polack PO. Chloride-mediated inhibition of the ictogenic neurones initiating genetically-determined absence seizures. *Neuroscience.* 2011;192:642-651.

60. Halász P, Terzano MG, Parrino L. Spike-wave discharge and the microstructure of sleep wake continuum in idiopathic generalised epilepsy. *Clin Neurophysiol.* 2002;32:38-53.

61. Zarowski M, Loddenkemper T, Vendrame M, Alexopoulos AV, Wyllie E, Kothare SV. Circadian distribution and sleep/wake patterns of generalized seizures in children. *Epilepsia.* 2011;52:1076-1083.

SUPPORTING INFORMATION

Additional supporting information can be found online in the Supporting Information section at the end of this article.